American Mineralogist, Volume 73, pages 754–765, 1988

Chemistry of biotites and muscovites in the Abas granite, northern Portugal

RUDY J. M. KONINGS,* JIM N. BOLAND,** SIMON P. VRIEND, J. BEN H. JANSEN
Department of Geochemistry and Experimental Petrology, State University of Utrecht, Budapestlaan 4, 3585 CD Utrecht, The Netherlands

ABSTRACT

The micas in the Abas granite (northern Portugal) have been examined by means of electron microprobe, scanning and transmission electron microscopy, and partial chemical analyses on mica separates. Four different types of postmagmatic muscovites are distinguished in thin sections, and their chemical variations are described in terms of celadonite, paragonite, and pyrophyllite substitutions. The paragonite substitution indicates that the four muscovite types formed at successively lower temperatures. Generally, the biotites exhibit texturally magmatic features, whereas they chemically have a deficient octahedral occupancy, suggesting considerable alteration to muscovite or zinnwaldite. Our observations suggest that the chemical variations in the biotite composition can more likely be explained by solid solution rather than by fine-scale intergrowths of the end-member minerals. Deficient interlayer occupancy of the biotites is caused at least in part by fine-scale interlayering of retrograde chlorite.

INTRODUCTION

Petrologic and geochemical investigation of Hercynian granitic rocks in central northern Portugal (Konings et al., 1988) indicated that large-scale metasomatic alteration of the Abas granite resulted in important changes in the whole-rock chemistry. A zone of tin-tungsten deposits is located near the contact with the younger Viseu granite (278 Ma; H.N.A. Priem, pers. comm.). Ten Haven et al. (1986) related part of the alteration and the tin-tungsten mineralization in the Abas granite to the intrusion of the Viseu granite.

The chemistry of the micas in the Abas granite is significant for the understanding of the whole-rock chemistry and the alteration processes. Replacement of biotite by muscovite has caused mobilization of refractory elements from the octahedral sheets and from the enclosed accessory minerals. In addition, the occurrence of secondary muscovite seems closely related to the alteration processes that were induced by the intrusion of the Viseu granite and its derivatives.

In the present study, the results of electron-microprobe analyses are interpreted in terms of either substitutional replacements or mica intergrowths. Supplementary chemical analyses of mica separates and scanning electron microscope (SEM) and transmission electron microscope (TEM) analyses were made to support these interpretations.

SAMPLING AND TECHNIQUE

The samples examined in this study were selected from 54 whole-rock samples collected from the Abas granite, both inside and outside the contact zone with the Viseu granite. The samples represent the various stages of alteration, which gradually increases toward the contact zone. Samples 04, 05, 07, 37, and 79 are heavily altered; 06, 25, and 80 are intermediate; 20 and 77 are less altered; and 29 has the most magmatic features. The sample locations and details of the petrology are described by Vriend, Konings, and Jansen (in prep.).

Most of the mineral analyses were made with a TPD electron microprobe at the University of Utrecht, operating at 15 kV and 4 nA, using energy-dispersive X-ray spectroscopy techniques.

The SEM and X-ray scanning images were made with a Cambridge Scientific Instruments Microscan M-9 at the Free University of Amsterdam (VU), operating at 20 kV and 25 nA, using wavelength-dispersive spectroscopy techniques. Some additional analyses that were made at the VU included fluorine. Natural and synthetic minerals were used as standards, and ZAF online full matrix corrections were applied according to the method used by Microscan. The resolution of the microprobe and the SEM analyses is 3–5 μm. The structural formulas were calculated on the basis of 22 oxygens.

Specimens for TEM were prepared by Ar thinning of grains selected from thin sections. The specimens were coated with C. Electron microscopy was performed with a JEM 200C microscope operated at 200 kV. Semiquantitative chemical analyses, with a spatial resolution of about 500 Å (i.e., the approximate beam size) were done with a Link X-ray analyzer using a C sample holder.

Mica fractions were separated from a selection of whole-rock samples by means of a Fault table, using the 30- to 50-μm fraction. The separation of biotite from muscovite was done with a Frantz electromagnetic separater, operated in steps of 0.2 mA. In general, several muscovite and biotite fractions were obtained from each sample, and all fractions were analyzed if the yield was large enough. Further purification was performed by means

* Present address: Netherlands Energy Research Foundation ECN, Department of Chemistry, P.O. Box 1, 1755 ZG Petten, The Netherlands.

** Present address: CSIRO, Division of Geomechanics, P.O. Box 54, Mount Waverley, Victoria 3149, Australia.

0003–004X/88/0708–0754$02.00

of heavy liquids. No feldspar or quartz impurities were observed after this treatment, but contamination of especially the biotite fraction as a result of fine-scale intergrowths with muscovite or chlorite could not be avoided. The separates were analyzed by ICPES (inductively coupled plasma-emission spectroscopy) after sample decomposition with a HF solution.

Petrologic observations

The Abas granite is a two-mica granite that locally grades into a muscovite granite. The bulk of the rock consists of quartz, plagioclase that has been mostly replaced by albite, and K-feldspar. Biotite is a primary magmatic constituent, frequently replaced by muscovite, tourmaline, and chlorite. The accessory minerals zircon, xenotime, and monazite are of primary origin, whereas sillimanite and rutile are secondary. Magmatic as well as postmagmatic apatite is present in minor amounts.

The biotite is dark brown and encloses a large number of accessory minerals, which are often obvious in thin section as a result of their nearly black pleochroic halos. During the muscovitization process, the pleochroic colors of biotite become pale brown, and the number of inclusions gradually decreases. During ubiquitous retrogradation, some biotite is altered to green biotite and chlorite.

Replacement textures suggest that muscovite is mainly of secondary origin. Four types of muscovite can be distinguished: (1) Large euhedral crystals apparently replace biotite and tourmaline. Partially resorbed inclusions of zircon, xenotime, and monazite, originally surrounded by biotite, are occasionally observed in these muscovite grains, and weakly colored pleochroic halos are rarely still recognizable in the muscovite matrix around these relicts. (2) Fine-grained sericite occurs as an alteration product of both magmatic and postmagmatic feldspar. (3) Fine-grained crystals occur along grain boundaries of type 1 muscovites or as aggregates in cracks. (4) Small crystals overgrow the other types of muscovite.

Muscovites of types 1 and 2 are ubiquitous and are related to the early and main alteration stages. Type 3 muscovites do not occur in the least altered zones, but are common in the areas where the alteration is more advanced. Type 4 muscovites are restricted to some intensely altered areas. Types 3 and 4 are related to the late alteration stages. Type 1 muscovite forms the greater part of the muscovite fraction in the rocks, whereas the amounts of type 2 and especially type 3 and 4 muscovites are relatively small. Consequently, the analyses of the muscovite separates mainly represent the type 1 composition.

Results and interpretation

Muscovite

Partial chemical analyses of the mica fractions are listed in Table 1. Normally, two relatively pure muscovite fractions were obtained, the amagnetic >1.5-mÅ fraction and the 1.3- to 1.5-mÅ fraction. The major difference between the two fractions is, of course, the Fe content, but the concentrations of the trace elements Li, Rb, and Cs also tend to be somewhat higher in the Fe-rich fraction, probably owing to minor biotite contamination. The concentrations of the trace elements Li, Rb, and Cs (Table 1) clearly increase with progressive alteration for muscovite as well as biotite.

Representative microprobe analyses of the four muscovite types are listed in Table 2. The variation diagrams of Si with respect to Al, Fe, and Mg as analyzed by microprobe (Fig. 1) show remarkable differences between the chemical compositions of the four muscovite types. Type 1 muscovite has relatively low Si and Mg contents and high Na and Al contents, whereas type 4 muscovite has high Si and Mg contents and very low Na, (K + Na + 2Ca), and Al contents. Types 2 and 3 have compositions intermediate between those of types 1 and 4. The Ti content of all muscovite types is extremely low and points toward postmagmatic origin (Speer, 1984), which is in agreement with our textural observations on the thin sections.

The variation of the Na content of the muscovites is attributed to solid solution between the end members muscovite and paragonite (Yoder and Eugster, 1955a, 1955b; Iijama, 1955). Recent studies by Chatterjee and Froese (1975) and Eugster et al. (1972) have provided useful information about the phase relations and their temperature dependence in this system. Discussing the possibilities for the use of the muscovite-paragonite system as a petrogenetic indicator in pelitic schists, Guidotti and Sassi (1976) and Guidotti (1984) argued that its applicability depends on the mineral assemblage. In the Abas granite, all muscovite types coexist with albite, quartz, and K-feldspar, and sillimanite is locally present. The Na content of the whole-rock samples increases with progressive alteration. This suggests that the altering fluids were rich in Na and were constantly buffered by the granitic mineral assemblage. It is concluded that the decreasing Na contents of muscovite types 1 to 4 must suggest a decrease of formation temperature. The Na_2O concentrations in the muscovite fractions (Table 1), which are dominated by type 1 muscovite, are fairly constant within each sample set representing rocks with the same degree of alteration, and the analytical results are comparable to the type 1 microprobe analyses.

The variation of Fe, Mg, and Al with Si (Fig. 1) can be related to solid solution between the end members muscovite and celadonite. The celadonite or Tschermak's substitution can be defined as

$$R^{3+} + {}^{[4]}Al = Si + R^{2+} \quad (1)$$

in which R^{3+} = Al,Fe and R^{2+} = Mg,Mn. Velde (1965, 1967) argued that in the system K_2O-MgO-Al_2O_3-SiO_2, substitution 1 is temperature and pressure dependent and the Si content of the muscovites could operate as an indicator of the conditions of formation. The applicability of this geothermometer is dependent on the buffering conditions during formation, i.e., the chemistry of the alterating fluids. The increasing (Fe_{tot} + Mg) from the

TABLE 1. Some major- and trace-element analyses of the mica separates

Sam.:	04	04	04	05	05	05	05	06	20	20	20	25	25
Type:	ms	ms	ms + bi	ms	ms	bi	bi	ms	ms	bi	bi	ms	ms
Magn.:*	>1.5	1.5–1.3	1.1–0.9	>1.5	1.5–1.3	0.7–0.5	0.5–0.3	>1.5	>1.5	0.7–0.5	0.5–0.3	>1.5	1.5–1.3
Alt.:	he	he	he	he	he	he	he	in	ls	ls	ls	in	in
Na_2O	0.67	0.57	0.44	0.51	0.28	0.05	0.05	0.39	0.42	0.07	0.04	0.46	0.31
FeO	1.59	2.19	4.07	1.60	2.25	17.74	20.88	1.18	1.07	14.50	18.44	1.61	2.07
Fe_2O_3	1.11	1.23	3.86	1.07	1.55	1.00	0.22	1.36	1.10	2.88	0.78	0.61	1.92
MgO	0.80	0.96	1.54	0.78	0.80	2.27	1.92	0.45	0.83	4.24	4.44	0.76	0.96
MnO	0.06	0.09	0.27	0.05	0.06	0.43	0.40	0.01	0.01	0.21	0.23	0.03	0.04
Li	1424	1922	4072	1549	1765	6207	4641	715	591	1890	1667	984	1402
Rb	1526	1726	1713	1364	1456	2700	2107	1912	686	1231	1130	1016	1268
Cs	127	219	496	128	286	1352	710	244	108	353	269	158	265
Ba	50	69	181	66	74	100	112	171	123	75	95	75	92
Sr	4	5	8	4	4	6	5	9	4	6	5	4	4

Note: Na_2O, FeO, Fe_2O_3, MgO, and MnO in weight percent; trace elements in ppm. Sam. refers to sample number; type refers to mineral type where ms is muscovite, bi is biotite, and chl is chlorite; and alt. refers to intensity of alteration where he means heavily, in means intermediate, ls means less, and mm means most magmatic.

* Magnetic interval in milliamperes on the Frantz magnetic separator.

type 1 to the type 4 muscovites is opposite to the trend in the whole-rock samples in which the MgO, FeO, and Fe_2O_3 concentrations steadily decrease with progressing alteration (Vriend, Konings, and Jansen, in prep). Consequently, no evidence is present for buffering of Fe_{tot} and Mg by a fluid during the alteration, and the muscovite-celadonite solid-solution series cannot be used as a petrogenetic indicator for the Abas granite. Nevertheless, the results would be consistent with the conclusions drawn from the paragonite-muscovite series. A Na–(Fe + Mg) avoidance in muscovite has already been suggested by Guidotti (1984) and Katagas and Baltatzis (1980), and it may be the cause of the observed consistency in this set of muscovites.

The negative correlation between (K + Na + 2Ca) and Si (Fig. 1) can be explained by a substitution involving interlayer vacancies,

$$K + {}^{[4]}Al = Si + V_A, \quad (2)$$

in which V_A represents a vacancy on the interlayer or A site, following the notation of Kröger (1985). As tetrahedral Al and Si are involved in this substitution, it causes significant deviations from the ideal celadonitic substitution. Because (Mg + Fe_{tot}) do not balance the excess Si in several Si-rich muscovites, significant deviations in the interlayer occupancy can be explained by substitution 2 rather than by the incorporation of the Rb, Cs, Sr, and Ba, which were analyzed in the bulk separates. The Sr and Ba concentrations in the muscovite fractions are relatively low. The Cs and especially the Rb concentrations are significantly higher, but the enrichment of these elements is related to the main alteration stage in the Abas granite and not to the late alteration stages during which the muscovites of types 3 and 4 were formed.

TABLE 2. Selection of 8 out of 70 chemical analyses of the four muscovite types (ms-1 to ms-4)

Type:	ms-1	ms-1	ms-1	ms-2	ms-2	ms-3	ms-3	ms-4
Sam.:	79	79	04	80	07	04	79	79
Alt.:	he	he	he	in	he	he	he	he
SiO_2	45.83	46.80	46.86	46.37	45.79	46.73	48.49	51.96
Al_2O_3	34.84	33.74	31.86	34.44	30.79	31.63	30.68	29.62
TiO_2	0.53	0.82	0.72	0.14	0.40	0.31	n.d.	n.d.
FeO	1.47	1.53	3.96	2.35	4.63	3.83	3.01	1.55
MnO	n.d.	n.d.	n.d.	n.d.	0.30	0.14	n.d.	n.d.
MgO	0.49	0.94	0.73	0.44	0.58	0.82	1.69	2.21
CaO	0.18	0.18	n.d.	0.31	n.d.	n.d.	0.18	0.27
Na_2O	0.92	0.60	0.16	0.62	n.d.	0.17	n.d.	n.d.
K_2O	9.98	10.12	10.83	10.30	10.61	10.71	10.58	9.49
Total	94.24	94.73	95.12	94.97	93.10	94.34	95.63	95.10
Si	6.166	6.261	6.340	6.219	6.358	6.368	6.535	6.834
$^{[4]}Al$	1.834	1.739	1.660	1.781	1.642	1.632	1.465	1.166
$^{[6]}Al$	3.693	3.582	3.422	3.666	3.399	3.450	3.410	3.428
Ti	0.054	0.083	0.074	0.014	0.042	0.032	—	—
Fe	0.166	0.171	0.445	0.265	0.538	0.437	0.340	0.171
Mn	—	—	—	—	0.036	0.017	—	—
Mg	0.099	0.189	0.148	0.090	0.122	0.168	0.340	0.434
Ca	0.027	0.027	—	0.046	—	—	0.026	0.038
Na	0.240	0.156	0.044	0.161	—	0.046	—	—
K	1.713	1.727	1.870	1.763	1.879	1.826	1.820	1.594
Total	13.992	13.935	14.003	14.005	14.016	13.976	13.936	13.665

Note: n.d. = not detected. For explanation of abbreviations, see Table 1.

TABLE 1—*Continued*

25	29	29	29	37	37	37
bi	ms	bi	bi	ms	ms	bi
0.7–0.5	>1.5	0.7–0.5	0.5–0.3	>1.5	1.5–1.3	0.7–0.5
in	mm	mm	mm	he	he	he
0.05	0.42	0.07	0.05	0.44	0.30	0.05
18.11	0.86	14.23	16.60	1.74	n.a.	10.66
2.49	0.68	3.70	1.26	1.27	n.a.	6.34
2.52	0.76	5.77	6.30	0.61	0.78	1.51
0.28	0.01	0.14	0.17	0.04	0.06	0.32
2325	229	1031	1134	1231	1890	3677
1483	600	1129	1226	1230	1582	2584
657	43	148	145	117	272	1094
39	226	121	129	94	72	59
8	10	5	4	5	4	7

Substitution 2 leads to the theoretical end member pyrophyllite. Velde (1969) examined the phase relations in the pseudobinary muscovite-pyrophyllite system at elevated temperatures and pressures. He suggested substantial solid solution in the muscovite-rich portion of the system. Our data indicate an increasing pyrophyllite substitution from type 1 to type 4 muscovite, which correlates with a decrease of the paragonite component and an increase of the celadonite component.

Figure 1 also shows a discontinuity in the relationships of Al and Fe with Si for eight Si-rich muscovites. These late muscovites deviate from the linear trend in the bulk of the analyses in having relatively high Al and low Fe_{tot} concentrations. Presumably a change occurred in the chemistry of the late alterating fluids that drastically affected the Fe^{3+}-^{VI}Al exchange.

If we assume that (1) Ca substitutes in the interlayer, compensated by a Si-$^{[4]}Al$ exchange, and Ti substitutes in the octahedral sheet and (2) all interlayer vacancies are due to substitution 2, then the number of divalent cations in the octahedral sheet can be approximated as $\frac{1}{4}[(Si - 6) - V_i - Ca - Ti]$. Likewise, the substitution parameters, expressed in percentage par, cel, and pyr, can be calculated. Figure 2 displays the distribution of the muscovites in the muscovite corner of a pyrophyllite–(muscovite + paragonite)–celadonite composition diagram. The type 1 muscovites plot near the muscovite end member, whereas types 2 and 3 and especially type 4 contain relatively high

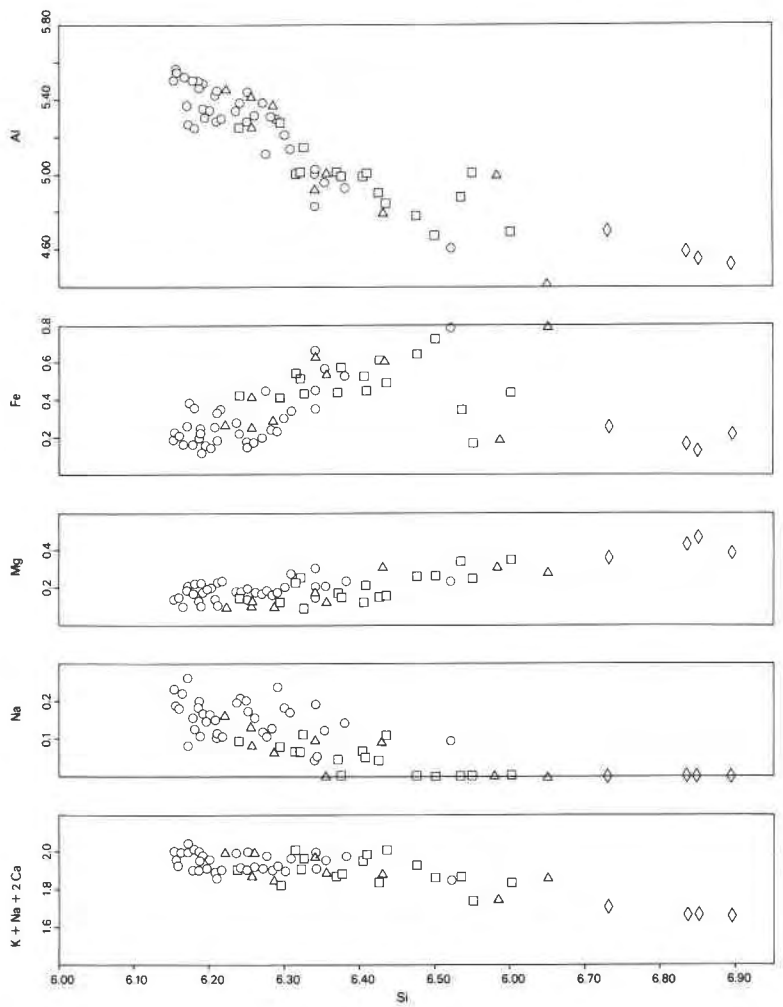

Fig. 1. Variation diagrams for Al, Fe, Mg, Na, and (K + Na + 2Ca) with Si in the four muscovite types. Circle = type 1, triangle = type 2, square = type 3, diamond = type 4.

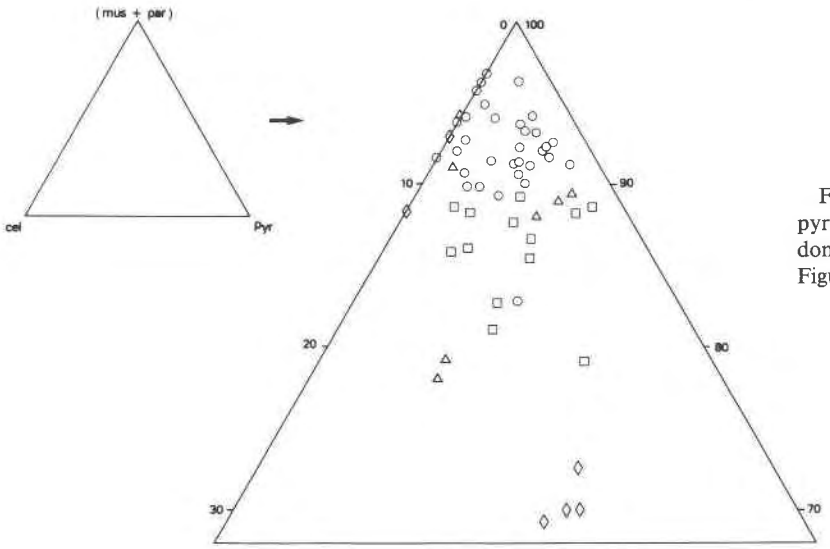

Fig. 2. Distribution of the muscovites on a pyrophyllite–(muscovite + paragonite)–celadonite composition diagram. Symbols as in Figure 1.

celadonite and pyrophyllite components, trending toward illite composition (Hower and Mowatt, 1966).

Biotite

Biotite microprobe analyses from the Abas granite deviate from the ideal composition in having a low total sum of cations (Table 3), which is caused by deficient octahedral or deficient interlayer occupancy.

In Figure 3, the Si, Al, (Fe_{tot} + Mg), and Ti contents of the biotites with a deficient octahedral occupancy and some deviating muscovites are plotted against the total sum of cations. A total sum of 14 represents a mean type 1 muscovite and a total sum of 16 represents a theoretical magmatic biotite (Albuquerque, 1973; Neiva, 1977). Between the Si, Ti, Al, (Fe_{tot} + Mg) contents of the deviating biotites and muscovites and the total sum of cations there exist clear relations (dashed lines) that are parallel to the predicted relations (straight lines) for the Al and (Fe + Mg) contents. The observed and predicted trends almost coincide for Si. After approximate corrections for the Fe^{3+}-Al exchange ($Fe^{3+} = Al_{predicted} - Al_{measured}$), the predicted and observed lines are in good agreement. Evidently, the Fe^{3+} content in the biotites is constant and not affected by the processes causing this chemical variation. The Fe_2O_3 concentrations in the mineral separates (Table 1) support this conclusion, although a clear difference in the Fe_2O_3 concentrations exists between the 0.7- to 0.5-mA and 0.5- to 0.3-mA fractions.

TABLE 3. Selection of 8 out of 62 chemical analyses of biotites and biotite-like material

Sam.:	07	25	25	25	25	29	29	77
Type:	bi	chl	bi + chl	bi + chl	bi	bi	bi	bi
Alt.:	he	in	in	in	in	mm	mm	ls
SiO_2	40.66	23.84	25.66	34.95	35.69	35.77	35.42	38.62
Al_2O_3	23.12	21.86	22.66	23.87	18.68	18.03	18.47	21.21
TiO_2	1.36	0.22	n.d.	n.d.	2.36	3.26	2.92	1.82
FeO	16.40	39.38	35.56	23.14	21.37	21.67	21.66	20.45
MnO	0.26	0.27	0.38	0.40	0.43	n.d.	0.23	0.68
MgO	1.02	2.30	2.91	2.72	6.15	7.01	7.40	1.86
CaO	n.d.	n.d.	n.d.	0.09	n.d.	n.d.	n.d.	n.d.
Na_2O	n.d.	n.d.	0.21	0.23	0.58	0.34	0.53	n.d.
K_2O	9.96	n.d.	0.18	2.68	9.24	9.19	9.04	9.86
Total	92.78	87.87	87.56	87.08	94.50	95.17	95.67	94.50
Si	6.123				5.535	5.491	5.429	5.889
$^{[4]}Al$	1.877				2.465	2.509	2.571	1.111
$^{[6]}Al$	2.228				0.950	0.754	0.767	2.700
Ti	0.155				0.276	0.377	0.337	0.209
Fe	2.066				2.771	2.782	2.777	2.609
Mn	0.033				0.058	—	0.031	0.089
Mg	0.230				1.423	1.604	1.691	0.425
Ca	—				—	—	—	—
Na	—				0.176	0.103	0.158	—
K	1.915				1.829	1.806	1.768	1.920
Total	14.627				15.483	15.426	15.529	14.952

Note: n.d. = not detected. For explanation of abbreviations, see Table 1.

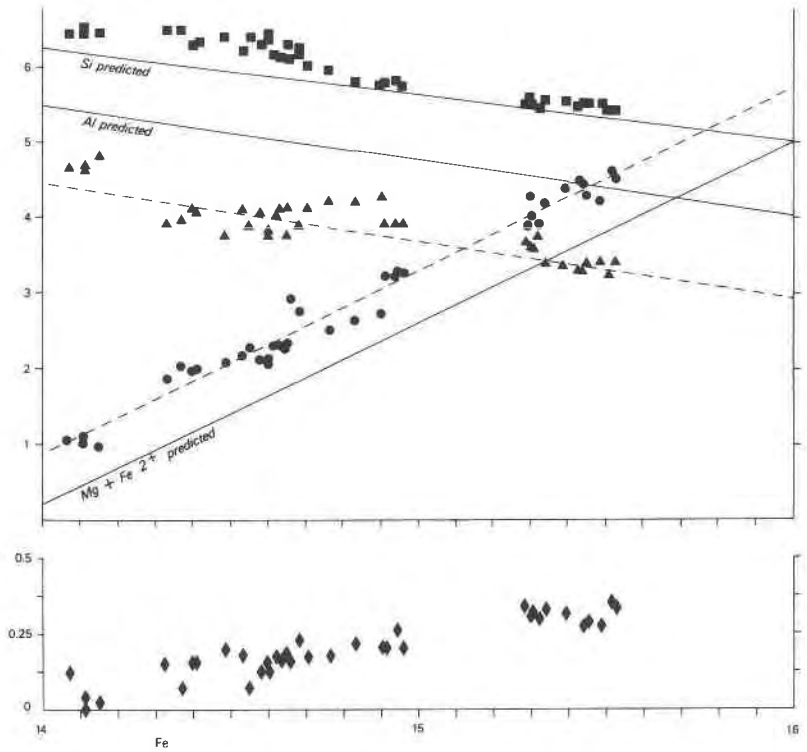

Fig. 3. The relationships between total sum of cations and Si (squares), Al (triangles), Fe_{tot} + Mg + Mn (circles), and Ti (diamonds). Symbols refer to altered and unaltered biotite, except those four with a total sum close to 14.1, which refer to muscovite.

All the data suggest extensive solid solution between muscovite and biotite that can be described by substitutions involving octahedral vacancies,

$$3R^{2+} = 2R^{3+} + V_R \quad (4)$$

$$2T^{3+} + R^{2+} = 2Si + V_R, \quad (5)$$

in which V_R represents a vacancy on the octahedral or R sites, R^{2+} = (Mn,Mg,Fe), T^{3+} and R^{3+} = (Al,Fe). Examination of data from natural and synthetic micas provided no clear indication of the permissible ranges of these substitutions (Crowley and Roy, 1964; Kwak, 1972; Rutherford, 1973; Robert, 1976; Green, 1981; Seifert and

TABLE 4. Chemical analyses of biotites and muscovites

Spot:*	AA	AB	AC	BA	BB	BC	BD	BE
Sam.:	25	25	25	05	05	05	05	05
Type:	bi	bi	ms	bi	bi	bi	ms	ms
Alt.:	in	in	in	he	he	he	he	he
SiO_2	35.10	34.90	45.00	38.80	37.60	37.20	41.20	44.30
Al_2O_3	19.90	20.30	34.50	23.50	23.10	23.30	22.60	28.40
TiO_2	3.01	2.47	0.61	1.56	1.88	1.79	1.06	1.55
FeO	24.00	23.90	1.80	17.00	18.30	18.30	14.20	6.21
MnO	0.31	0.25	n.d.	0.35	0.41	0.43	0.32	0.07
MgO	3.05	3.23	0.84	1.17	1.01	1.29	1.25	1.03
CaO	n.d.	n.d.	n.d.	n.d.	n.d.	n.d.	n.d.	n.d.
Na_2O	0.08	0.09	0.72	0.04	0.04	0.04	n.d.	0.11
K_2O	9.44	9.39	10.70	9.95	9.69	9.85	10.30	11.00
F	0.93	1.18	0.46	2.36	4.19	2.34	3.40	1.04
O≡F	−0.39	−0.50	−0.19	−0.99	−1.76	−0.99	−1.43	−0.44
Total	95.43	95.21	94.44	93.74	94.46	93.55	92.90	93.27
Si	5.480	5.460	6.100	5.930	5.810	5.760	6.270	6.290
[4]Al	2.520	2.540	1.900	2.070	2.190	2.240	1.730	1.710
[6]Al	1.140	1.210	3.610	2.150	2.020	2.000	2.310	3.030
Ti	0.353	0.291	0.062	0.180	0.219	0.208	0.122	0.166
Fe	3.140	3.120	0.205	2.170	2.370	2.370	1.810	0.738
Mn	0.040	0.033	—	0.045	0.054	0.056	0.042	0.008
Mg	0.709	0.754	0.170	0.266	0.233	0.298	0.284	0.219
Ca	—	—	—	—	—	—	—	—
Na	0.023	0.029	0.190	0.011	0.011	0.011	—	0.030
K	1.880	1.880	1.860	1.940	1.920	1.950	2.010	1.990
Total	15.285	15.317	14.097	14.762	14.827	14.893	14.578	14.181
F	0.459	0.584	0.197	1.140	2.050	1.150	1.640	1.040

Note: n.d. = not detected. For explanation of abbreviations, see Table 1.
* Spots labeled by letters as indicated in Figure 4.

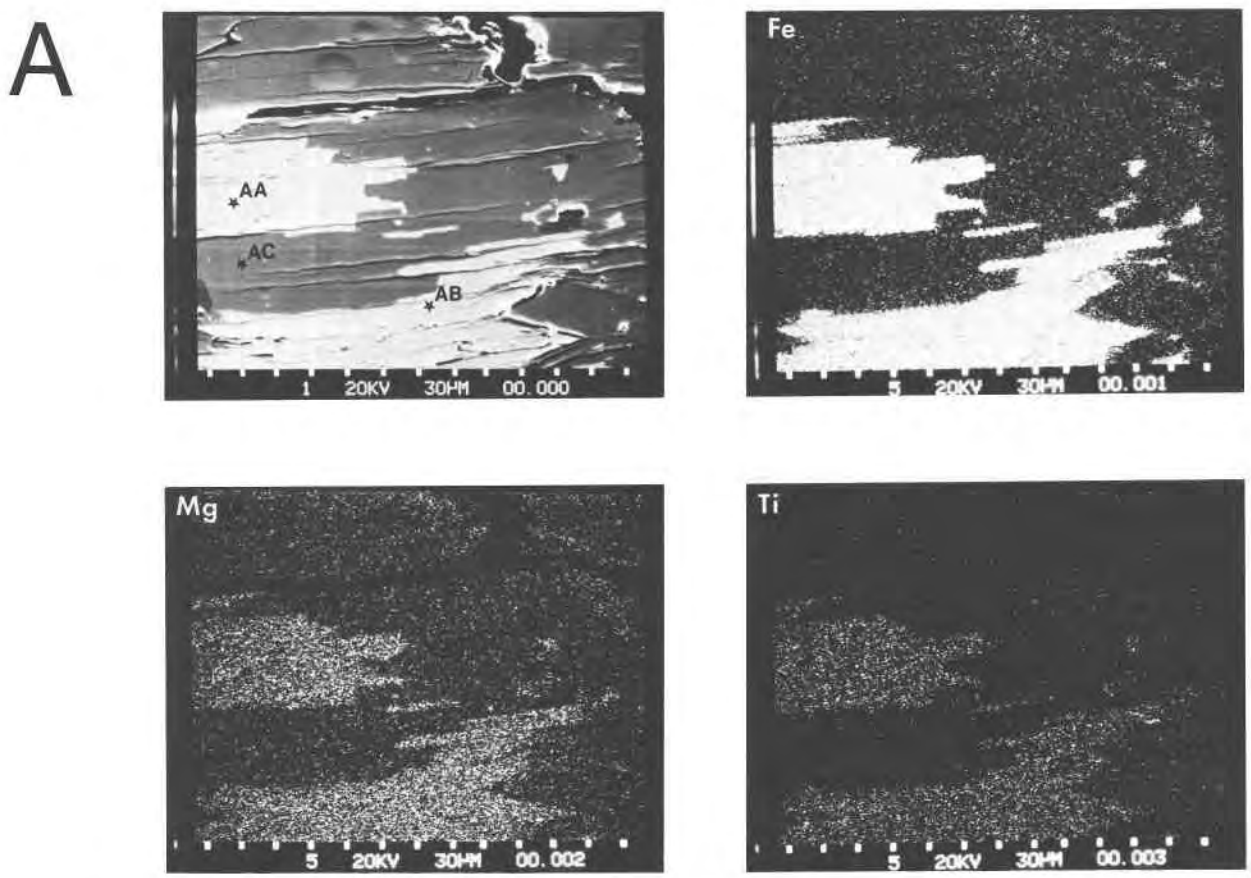

Fig. 4. SEM images and characteristic X-ray scanning images of biotite and muscovite grains of (**A**) sample 25 and (**B**) sample 05. Analyses from the indicated spots are presented in Table 4. The counting time for Fe in sample 25 is a third of that for sample 05. During the exposure, some of the C coating of sample 05 disappeared from the biotite grain in the left-bottom part of the photograph. Scale: 30 μm between adjacent white squares indicated at the bottom of each photograph.

Schreyer, 1965, 1971), but they certainly do not occur on such a large scale as suggested in Figure 3.

Figure 4 displays SEM images in combination with characteristic scanning maps for Fe, Mg, and Ti in muscovite and biotite grains. In sample 25 (Fig. 4A), clear differences exist in the concentrations of Fe, Mg, and Ti of both minerals. In sample 05 (Fig. 4B), almost no difference in Mg and Ti content can be observed, but there is still a distinct difference in Fe content of the minerals. Chemically, the minerals are rather homogeneous. Microprobe analyses of the same grains are listed in Table 4. The grains in sample 05 (Fig. 4B) have a remarkably high F content, up to 4.19 wt%, and they display a very low octahedral occupancy.

Another explanation for the deficient octahedral occupancy is the substitution of Li, which cannot be analyzed for by electron-microprobe techniques. The principal Li substitutions can be expressed as

$$2R^{2+} = Li + {}^{[6]}Al \quad (6)$$

$$R^{2+} + {}^{[4]}Al = Li + Si. \quad (7)$$

These substitutions are related to incorporation of zinnwaldite and lepidolite components. The pure minerals occur mainly in pegmatites and hydrothermal veins or as metasomatic alteration products of biotite (Deer et al., 1962; Černý and Burt, 1984). Both minerals may contain a considerable amount of F. A hydrothermal replacement of OH by F in micas is reviewed by Munoz (1984). Postmagmatic processes have strongly affected the whole-rock chemistry of the Abas granite and enrichment of Li, Rb, Cs, and F, among others, has been established (Vriend, Konings, and Jansen, in prep). Oen (1958) proved the presence of Li in micas of altered zones of the Abas granite by means of qualitative spectroscopic determination. Our chemical analyses of the mineral separates (Table 1) yield Li concentrations up to 6207 ppm in the biotite fractions. However, these amounts cannot totally account for the deficient octahedral occupancy as is evidenced by Figure 3. The biotite systematically contains more Li than the coexisting muscovite. The biotites in heavily altered samples contain 3677 to 6207 ppm Li, whereas those from less altered samples contain 1031 to 2325 ppm Li.

Apart from the substitutions discussed above, the chemical variations can be caused by interlayering and

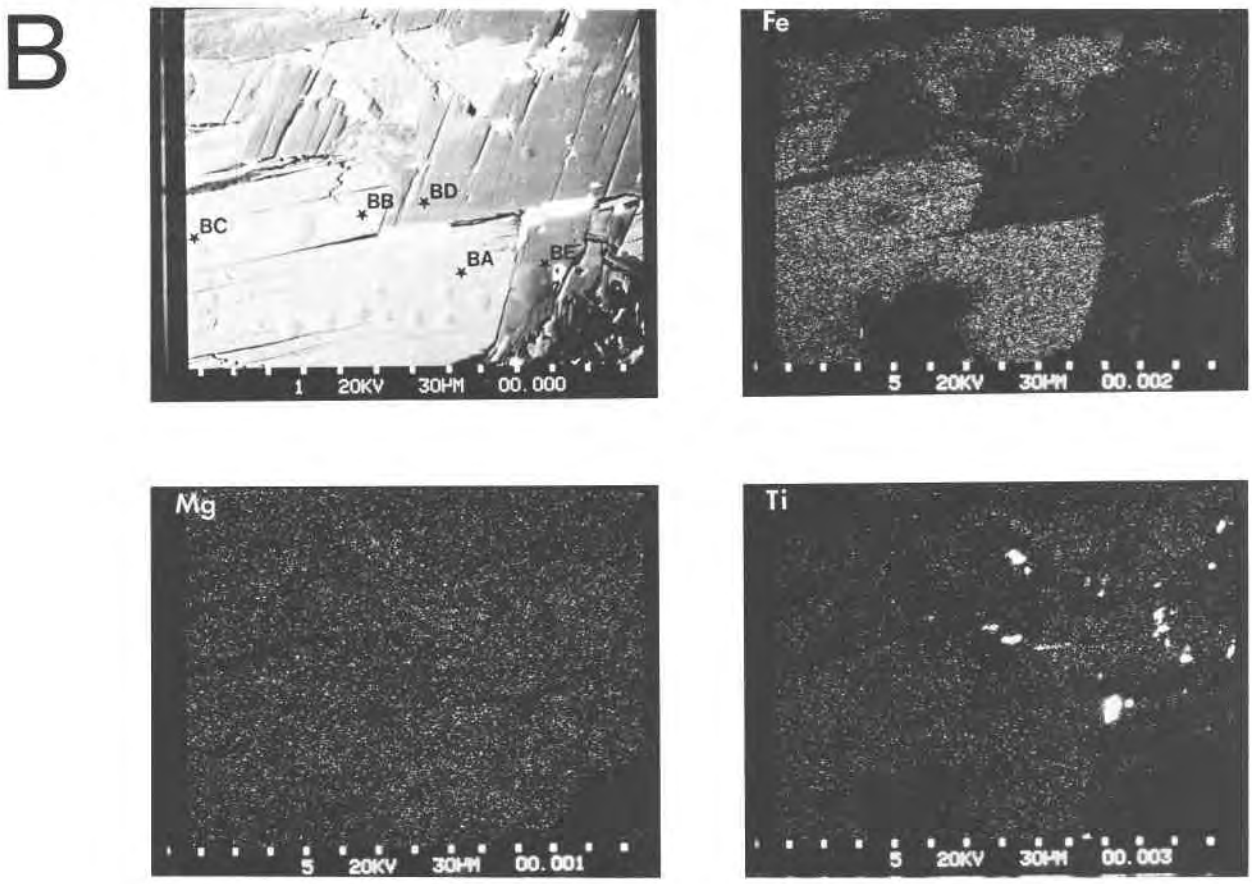

Fig. 4—*Continued.*

intergrowth of sheet silicates on a scale smaller than the resolution of the electron microprobe (spot size 3–5 μm). The muscovite-biotite interface of the grains in Figure 4A (sample 25) was also examined in some detail by TEM. The interface itself was not clearly defined. It consisted of thin bands several hundred ångströms wide of retrograde chlorite and a sheet silicate tentatively identified as smectite. The electron-diffraction pattern and the lattice image from the muscovite side of the interface exhibited sharp diffraction spots with a (001) repeat distance of 20 Å, consistent with a perfect $2M_1$ polytype viewed along [100] (Fig. 5). The lattice image consisted of fringes with a dominant periodicity of 20 Å. However, an intermediate 10-Å spacing was observed in certain more favorably oriented parts of the sample. The biotite had greater variability in its microstructure and diffraction pattern. Using bright-field TEM imaging, the biotite consisted of various irregularly spaced planar and lamellar structures superimposed on a series of 10-Å fringes (Figs. 6A, 6B). The diffraction pattern (Fig. 6C) indicated that the basic repeat unit was 10 Å with superlattice reflections corresponding to 30 Å, indicating that *1M* and possibly *3T* polytypes are present. The streaking between the dominant spots indicates that these polytypes are irregularly interlayered or that they possess abundant stacking faults (Iijima and

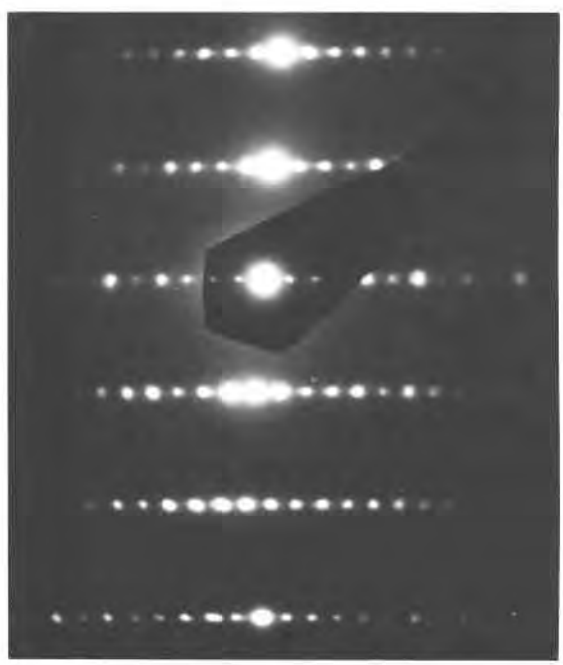

Fig. 5. Electron-diffraction pattern of muscovite from sample 25.

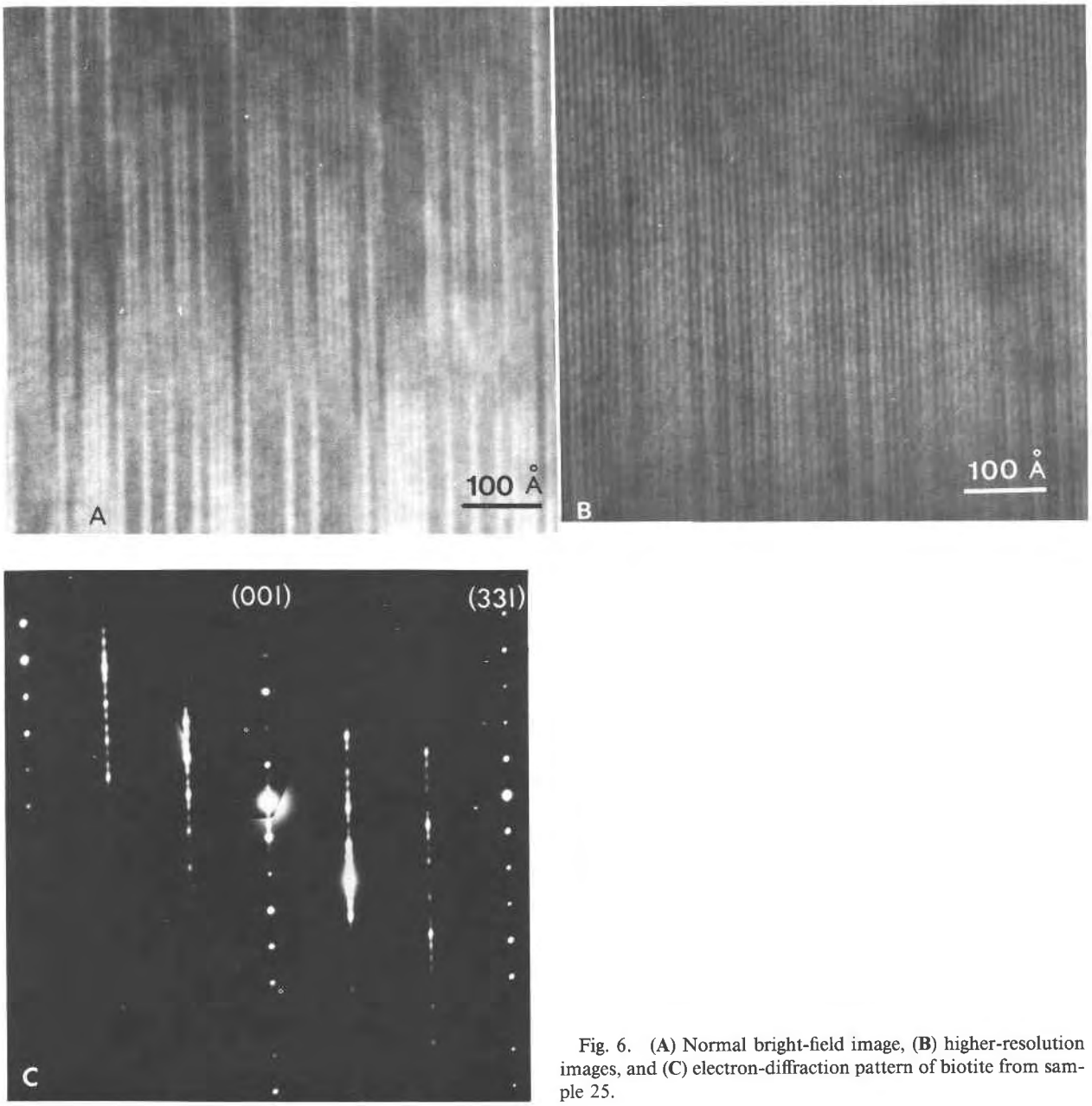

Fig. 6. (**A**) Normal bright-field image, (**B**) higher-resolution images, and (**C**) electron-diffraction pattern of biotite from sample 25.

Zhu, 1982; Iijima and Buseck, 1978; Bell and Wilson, 1977). Extensive disordering and polytypism are observed in the biotite grains of Figure 4B (sample 05), in which the layer fringes in the biotite often appear to be discontinuous and distorted.

Using the semiquantitative X-ray analytical capability of the TEM, it was established that in both samples, no significant chemical variations were associated with the stacking disorder in the biotite. This homogeneity indicates that the lamellae are chemically identical and that no distinct intergrowths can be observed on a scale of several hundred ångströms.

In the muscovite section, the interlayer deficiency of micas was discussed in terms of substitutions involving vacancies. The incorporation of Sr on the interlayer site of biotite is negligible, and that of Ba does not exceed 129 ppm in the most magmatic sample (Table 1). Although high Rb and Cs contents of 2700 ppm and 1352 ppm, respectively, were determined in biotite fractions of the heavily altered samples, for most biotites the interlayer deficiency is not compensated by these amounts. Many biotite compositions with a calculated low interlayer occupancy appeared to be green biotite, occasionally intergrown with chlorite (Table 3). We prefer to relate these compositions to replacement by chlorite and kaolinite, which form during retrograde low-temperature al-

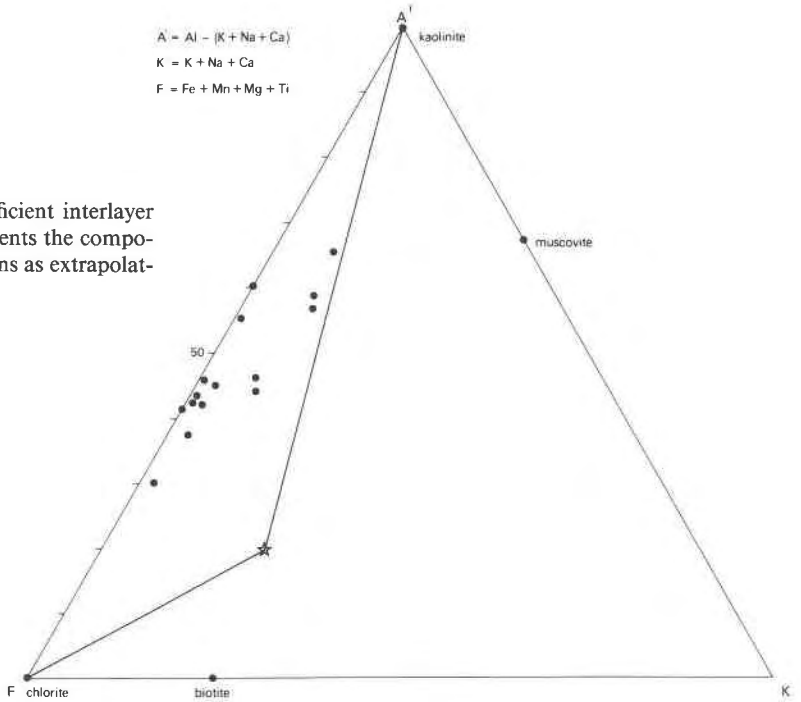

Fig. 7. Distribution of the biotites with deficient interlayer occupancy in a A′ KF-diagram. The star represents the composition of hypothetical biotite with 16 total cations as extrapolated on the variation diagram of Figure 3.

teration and weathering (Meunier and Velde, 1979; Craw et al., 1982; Cathelineau, 1983; Ahn and Peacor, 1987; Konings et al., 1988). In Figure 7, these biotite analyses of the Abas granite are plotted on an AKF diagram. Most analyses with low interlayer occupancy fall near the chlorite-kaolinite join, and the intermediate compositions suggest strong kaolinization of biotite.

However, only evidence for interlayering of chlorite in biotite is registered in the TEM images. Fringes with 14- or 28-Å spacings are observed in the biotites (Fig. 8) and can be explained by the presence of brucite layers (Veblen and Buseck, 1981; Veblen and Ferry 1983; Olives et al., 1983; Olives and Amouric, 1984; Olives, 1985). Such intercalations can account for the observed K depletion in several biotite analyses. The mechanism of chloritization in natural micas can be described by the replacement of TOT (tetrahedral-octahedral-tetrahedral) layers by brucite layers or by the replacement of the interlayer by a brucite layer (Veblen and Ferry, 1983; Olives and Amouric, 1984). From the present observations, it is not possible to distinguish which mechanism occurred in our samples.

Conclusions

1. The muscovites in the Abas granite are of postmagmatic origin and can be divided into four types on the basis of petrologic observations.

2. Microprobe analyses indicate that three important substitutions govern the muscovite composition:

$$R^{3+} + {}^{[4]}Al = R^{2+} + Si$$
$$K + {}^{[4]}Al = Si + V_A$$
$$K = Na.$$

These substitutions relate muscovite compositions to the celadonite, pyrophyllite, and paragonite end members, respectively.

3. The paragonite substitutions suggest that the four muscovite types crystallized successively as the temperature decreased. The muscovite types that developed lat-

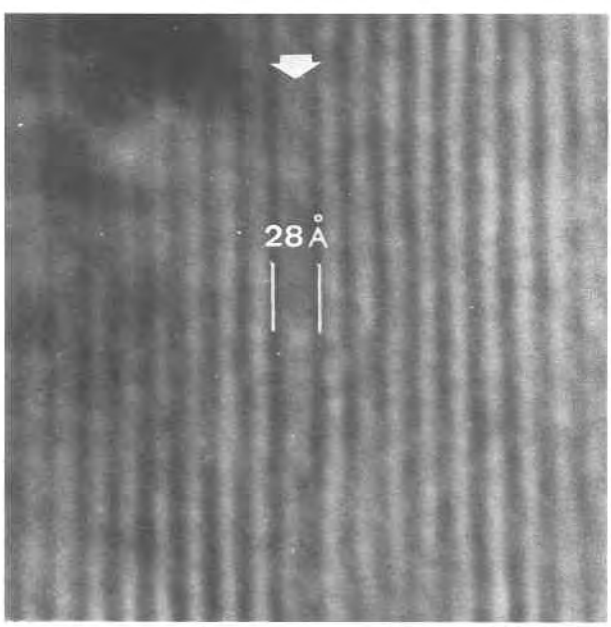

Fig. 8. Lattice image of biotite from sample 25. Arrow indicates a 28-Å fringe, presumably the result of intercalated chlorite.

er show increased pyrophyllite and celadonite substitutions.

4. The deficient octahedral occupancy of the biotites is probably due to postmagmatic hydrothermal alteration to form muscovite and zinnwaldite components.

5. The nature of the replacement mechanisms in biotite has not been definitively established. Since no textural intergrowths have been observed on a scale of several hundred ångströms with the methods employed in this study, a substitution mechanism seems likely, but interlayering on a smaller scale cannot be ruled out.

6. The deficient interlayer occupancy of the originally magmatic biotites is caused at least in part by fine-scale intercalation of retrograde chlorite and presumably kaolinite.

7. The Li, Rb, and Cs contents of the mica separates of the Abas granite increase with intensity of hydrothermal alteration, whereas their Ba (and MgO) contents decrease.

Acknowledgments

The electron-microprobe analyses and the transmission electron microscopy were performed with financial and personnel support by ZWO-WACOM (research group for analytical chemistry of minerals and rocks, subsidized by the Netherlands Organisation for Advancement of Pure Research). M. van Bergen and W. Lustenhouwer are thanked for their assistance with the analyses in Utrecht and Amsterdam, respectively. M. Amouric, M. van Bergen, J. T. Cheney, P. Hartman, and D. R. Veblen critically reviewed the manuscript and gave valuable comments for substantial improvement.

References cited

Ahn, J.H., and Peacor, D.R. (1987) Kaolinization of biotite: TEM data and implications for an alteration mechanism. American Mineralogist, 72, 353–356.

Albuquerque, C.A.R. de (1973) Geochemistry of biotites from granitic rocks, northern Portugal. Geochimica et Cosmochimica Acta, 47, 1223–1236.

Bell, I.A., and Wilson, C.J.L. (1977) Growth defects in metamorphic biotite. Physics and Chemistry of Minerals, 2, 153–169.

Cathelineau, M. (1983) Potassic alteration in French hydrothermal uranium deposits. Mineralium Deposita, 18, 89–97.

Černý, P., and Burt, D.M. (1984) Paragenesis, crystallochemical characteristics, and geochemical evolution of micas in granite pegmatites. Mineralogical Society of America Reviews in Mineralogy, 13, 257–298.

Chatterjee, N.D., and Froese, E. (1975) A thermodynamic study of the pseudobinary join muscovite-paragonite in the system $KAlSi_3O_8$-$NaAlSi_3O_8$-Al_2O_3-SiO_2-H_2O. American Mineralogist, 60, 985–993.

Craw, D., Coombs, D.S., and Kawachi, Y. (1982) Interlayered biotite-kaolinite and other altered biotites, and their relevance to the biotite isograd in eastern Otago, New Zealand. Mineralogical Magazine, 45, 79–85.

Crowley, M.S., and Roy, R. (1964) Crystalline solubility in the muscovite and phlogopite groups. American Mineralogist, 49, 348–362.

Deer, W.A., Howie, R.A., and Zussman, J. (1962) Rock-forming minerals, vol. 3 (Sheet silicates). Longman, London, 270 p.

Eugster, H.P., Albee, A.L., Bence, A.E. Thompson, J.B., and Waldbaum, D.R. (1972) The two-phase region and excess mixing properties of paragonite-muscovite crystalline solutions. Journal of Petrology, 13, 147–179.

Green, T.H. (1981) Synthetic high-pressure micas compositionally intermediate between the dioctahedral and trioctahedral mica series. Contributions to Mineralogy and Petrology, 78, 452–458.

Guidotti, C.V. (1984) Micas in metamorphic rocks. Mineralogical Society of America Reviews in Mineralogy, 13, 357–468.

Guidotti, C.V., and Sassi, F.P. (1976) Muscovite as a petrogenetic indicator mineral in pelitic schists. Neues Jahrbuch für Mineralogie Abhandlungen, 127, 97–142.

Haven, H.L. ten, Konings, R., Schoonen, M.A.A., Jansen, J.B.H., Vriend, S.P., Weijden, C.H. van der, and Buitenkamp, J. (1986) Geochemical studies in the drainage basin of the Rio Vouga (Portugal): II. A model for the origin of hydrothermal water in the Vouzela region. Chemical Geology, 51, 225–238.

Hower, J., and Mowatt, T.C. (1966) The mineralogy of illites and mixed-layer illite/montmorillonites. American Mineralogist, 51, 825–854.

Iijima, J.T. (1955) Etude des réaction d'échange d'ions Na-K dans la série muscovite-paragonite. Bullétin de la Société Française de Minéralogie et Cristallographie, 87, 532–541.

Iijima, S., and Buseck, P.R. (1978) Experimental study of disordered mica structures by high resolution electron microscopy. Acta Crystallographica, A34, 709–719.

Iijima, S., and Zhu, J. (1982) Electron microscopy of a muscovite-biotite interface. American Mineralogist, 67, 1195–1205.

Katagas, C., and Baltatzis, E. (1980) Coexisting celadonite, muscovite and paragonite in chlorite-zone metapelites. Neues Jahrbuch für Mineralogie Monatshefte, 5, 206–214.

Konings, R.J.M., Pinto, M.S., Jansen, J.B.H., and Vriend, S.P. (1988) Whole rock chemistry and element mobility in granitic rocks. Geologie en Mijnbouw, in press.

Kröger, F.A. (1985) Point defects in solids: Physics, chemistry and thermodynamics. In R.N. Schock, Ed., Point defects in minerals, pp. 1–17. American Geophysical Union Geophysical Monograph 31.

Kwak, T.A.P. (1972) An experimental study on Fe-Mg micas transitional between dioctahedral and trioctahedral compositions. Neues Jahrbuch für Mineralogie, 47, H7, 326–335.

Meunier, A., and Velde, B. (1979) Weathering mineral facies in altered granites: The importance of local small-scale equilibria. Mineralogical Magazine, 43, 261–268.

Munoz, J.L. (1984) F-OH and Cl-OH exchange in micas with applications to hydrothermal ore deposits. Mineralogical Society of America Reviews in Mineralogy, 13, 469–493.

Neiva, A.M.R. (1977) Distribution of some elements between coexisting minerals from granites, aplites and pegmatites from central northern Portugal. Chemical Geology, 20, 223–233.

Oen, I.S. (1958) The geology, petrology and ore deposits of the Viseu region, Northern Portugal. Communios Servicios Geologicos Portugal, 41, 5–199.

Olives, J. (1985) Biotites and chlorites as interlayered biotite-chlorite crystals. Bulletin de Minéralogy, 108, 635–641.

Olives, J., and Amouric, M. (1984) Biotite chloritization by interlayer brucitization as seen by HRTEM. American Mineralogist, 69, 869–871.

Olives, J., Amouric, M., De Fouquet, C., and Baronnet, A. (1983) Interlayering and interlayer slip in biotite as seen by HRTEM. American Mineralogist, 68, 754–758.

Robert, J.L. (1976) Phlogopite solid solutions in the system K_2O-MgO-Al_2O_3-SiO_2-H_2O. Chemical Geology, 17, 213–227.

Rutherford, M.J.G. (1973) The phase relations of aluminous iron biotites in the system $KAlSi_3O_8$-$KAlSiO_4$-Al_2O_3-Fe-O-H. Journal of Petrology, 14, 159–180.

Seifert, F., and Schreyer, W. (1965) Synthesis of a new mica, $KMg_{2.5}(Si_4O_{10})(OH)_2$. American Mineralogist, 50, 1114–1118.

——— (1971) Synthesis and stability of micas in the system K_2O-MgO-SiO_2-H_2O and their relation to phlogopites. Contributions to Mineralogy and Petrology, 30, 196–215.

Speer, J.A. (1984) Micas in igneous rocks. Mineralogical Society of America Reviews in Mineralogy, 13, 229–356.

Veblen, D.R., and Buseck, P.R. (1981) Hydrous pyriboles and sheet silicates in pyroxene and uralites: Intergrowth microstructures and reaction mechanisms. American Mineralogist, 66, 1107–1134.

Veblen, D.R., and Ferry, J.M. (1983) A TEM study of the biotite-chlorite reaction and comparison with petrological observations. American Mineralogist, 68, 1160–1168.

Velde, B. (1965) Phengitic micas: Synthesis, stability and natural occurrence. American Journal of Science, 263, 886–913.

——— (1967) Si^{4+}-content of natural phengites. Contributions to Mineralogy and Petrology, 14, 250–258.
——— (1969) The compositional muscovite-pyrophyllite at moderate pressure and temperatures. Bullétin de la Société Française de Minéralogie et Cristallographie, 92, 360–368.
Yoder, H.S., and Eugster, H.P. (1955a) Synthetic and natural muscovites. Geochimica Cosmochimica Acta, 8, 225–280.
——— (1955b) The join muscovite-paragonite. Carnegie Institution of Washington Year Book 54, 124–126.

Manuscript received July 15, 1985
Manuscript accepted February 29, 1988